Materials and Design 55 (2014) 325–334

Contents lists available at ScienceDirect

Materials and Design

journal homepage: www.elsevier.com/locate/matdes

Constitutive modeling and the effects of strain-rate and temperature on the formability of Ti–6Al–4V alloy sheet

Xiaoqiang Li *, Guiqiang Guo, Junjie Xiao, Nan Song, Dongsheng Li

School of Mechanical Engineering and Automation, Beihang University, Beijing 100191, China

ARTICLE INFO

Article history:
Received 13 June 2013
Accepted 27 September 2013
Available online 9 October 2013

Keywords:
Ti–6Al–4V alloy
Constitutive model
Forming limit diagram
Theoretical prediction
Strain-rate and temperature sensitivity

ABSTRACT

The constitutive model considering the strain-rate and temperature effects was presented by fitting the true stress–strain curves of Ti–6Al–4V alloy over a wide range of strain-rates (0.0005–0.05 s^{-1}) and temperatures (923–1023 K). The Forming Limit Curve (FLC) of Ti–6Al–4V alloy at 973 K was measured by conducting the hemispherical dome test with specimens of different widths. The forming limit prediction model of Ti–6Al–4V alloy, which takes strain-rate and temperature sensitivity into account, was predicted based on Marciniak and Kuczynski (M–K) theory along with Von Mises yield criterion. The comparison shows that the limit strain decreases with temperature lowering but strain-rate increasing. The comparison between theoretical analysis and experiment of FLC verifies the accuracy and reliability of the proposed methodology, which considers the strain-rate and temperature effects, to predict limit strains in the positive minor strain region of Forming Limit Diagram (FLD).

1. Introduction

Since the emergence of titanium and its alloys in the early 1950s, they have been extensively used in aerospace, defense, energy and medical industries [1]. For example, titanium and its alloys have been widely utilized in the aerospace components such as structural airframe and engine components, because of the excellent strength to weight ratio, outstanding resistance to corrosion and inherent thermal compatibility with composite materials [2]. Additionally, the application of titanium in medicine, such as artificial joints and dental implants, is more and more extensive [1]. This is mainly because of its excellent properties, such as high strength, light weight, resistance to corrosion, bio-compatibility and low modulus [3].

However, the formability of titanium alloys is unsatisfactory at room temperature. Compared with other traditional metallic materials, titanium alloy components are more difficult to form. They exhibit a high degree of springback, and the lower formability causes the material to crack or tear easily during forming processes at room temperature [4].

Therefore, there is increasing attention and interest to investigate the formability of titanium alloys [5]. Several studies have been performed to research the formability of titanium alloys at room temperature. Lang et al. investigated the cold forming behavior of Ti–15–3–3–3 based on simulation and experimental verification [6]. A numerical simulation method was developed by Jurendić et al. for the deep drawing process of α-titanium alloy sheet using LS-Dyna [7]. Esfahlan et al. investigated a new method of deep drawing assisted by floating disk for Ti–6Al–4V both in experimental and simulation [8]. Satoh et al. investigated the ability and behavior of two kinds of pure titanium and one of its alloy in the stretch-drawing process [9]. It is observed that the formability of titanium alloy sheets could be greatly improved by hot forming. Lai et al. investigated the effects of tooling temperatures on the formability of Ti-TWBs at elevated temperature. The results revealed that the formability of Ti-TWBs can be enhanced by elevated tooling temperatures [10]. It was found that the formability of both the Ti-TWBs and their base metal increases with increasing forming temperature in the study of Cheng et al. [11]. In the study of Chen and Chiu, the formability of commercially pure titanium sheets at various temperatures was studied by the experimental approach. The results obtained from the V-bend tests revealed that springback can be reduced at elevated forming temperature [12]. The experimental results from Lai et al. revealed that the ductility of Ti–6Al–4V was enhanced at higher working temperatures, because of a decrease in the yield strength [13]. In the study of Odenberger et al., a set of material tests were performed on Ti–6Al–4V at temperatures ranging from room temperature up to 833 K. The result indicated that the alloy can be formed to higher strain values at 673 K than at room temperature before fracture occurs [14]. Odenberger et al. also indicated that Ti-6242 is suitable to be formed by hot sheet metal forming [15]. However, this process increases the manufacturing cost. Finite element analysis has enjoyed considerable success and popularity in sheet metal forming analyses since

* Corresponding author. Tel.: +86 10 82316584.
E-mail address: lixiaoqiang@buaa.edu.cn (X.Q. Li).

0261-3069/$ - see front matter © 2013 Elsevier Ltd. All rights reserved.
http://dx.doi.org/10.1016/j.matdes.2013.09.069

its introduction. The accuracy and usefulness of simulation depends to a great degree on the accuracy of constitutive model used.

The forming limit, which reflects the largest deformation of the sheet metal before plastic instability, is used to quantitatively describe the formability of sheet metal [16]. It is a significant performance index and process parameter in the field of sheet metal forming. Forming Limit Diagram (FLD), which is introduced by Keeler and Goodwin, is a useful tool to evaluate the formability of different materials [17]. However, the experimental measurement of FLD is a difficult, time consuming and expensive process, especially at elevated temperature. Consequently, considerable effort has been made to construct reliable forming limit prediction models from the perspective of theoretical calculation. Recently several studies have been reported on the constitutive modeling and the formability predictions at elevated temperature using the theoretical Forming Limit Curves (FLCs). In the investigation of Min et al., a prediction model for hot forming limits of steel 22MnB5 was derived based on Storen and Rice's Vertex theory and Logan–Hosford yield criterion, and a calculation model was also established based on Logan-Hosford yield criterion according to Marciniak and Kuczynski (M–K) theory [18]. The FLDs of aluminum alloy 5083 were constructed from the perspective of theoretical calculation and finite element simulation, and the effect of the rate sensitivity index on its formability was evaluated by Zhang et al. [19]. In the study of Khan et al., M–K theory was used to obtain the theoretical strain and stress-based FLCs of AA5182-O at different strain-rates and temperatures [20]. Haghdadi et al. investigated the flow stress behavior of cast A356 aluminum alloy by a set of isothermal hot compression tests. The influence of strain was incorporated in an Arrhenius-type constitutive equation by considering the related material constants as functions of strain [21]. An artificial neural network model was established to estimate the high temperature flow behavior of a cast A356 aluminum alloy [22]. However, much research needs to be done on the forming limit prediction model of Ti–6Al–4V alloy, and the effects of strain-rate and temperature need to be further discussed.

This paper is focusing on the method to obtain theoretical FLC using the Backofen equation, which takes strain-rate and temperature sensitivity into account. The forming limit prediction model is based on M–K theory along with Von Mises yield criterion. Then, the effects of strain-rate and temperature on the formability of Ti–6Al–4V alloy are discussed. The comparison between theoretical FLC and experimental FLC is used to verify the reliability and robustness of the prediction.

Table 1
Chemical composition of as-received Ti–6Al–4V alloy (wt.%).

Material	Al	V	Fe	C	H	O	Ti
Ti–6Al–4V	6.02	3.78	0.08	0.007	0.0082	0.074	Bal.

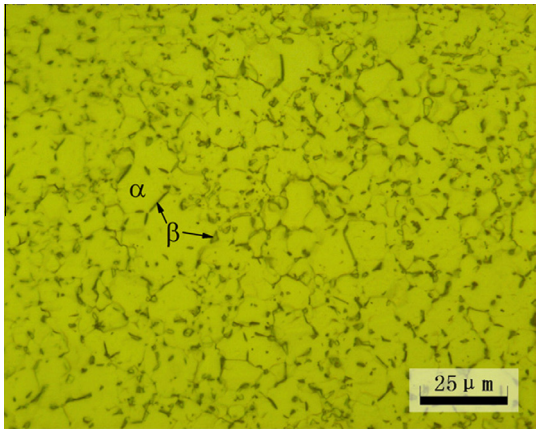

Fig. 1. Initial microstructure of the Ti–6Al–4V alloy sheet [23].

2. Experimental procedures

2.1. Material

The chemical composition of Ti–6Al–4V alloy is listed in Table 1. The as-received alloys were annealed after hot and cold rolling into sheet of 1.5 mm thickness. The initial microstructure is shown in Fig. 1.

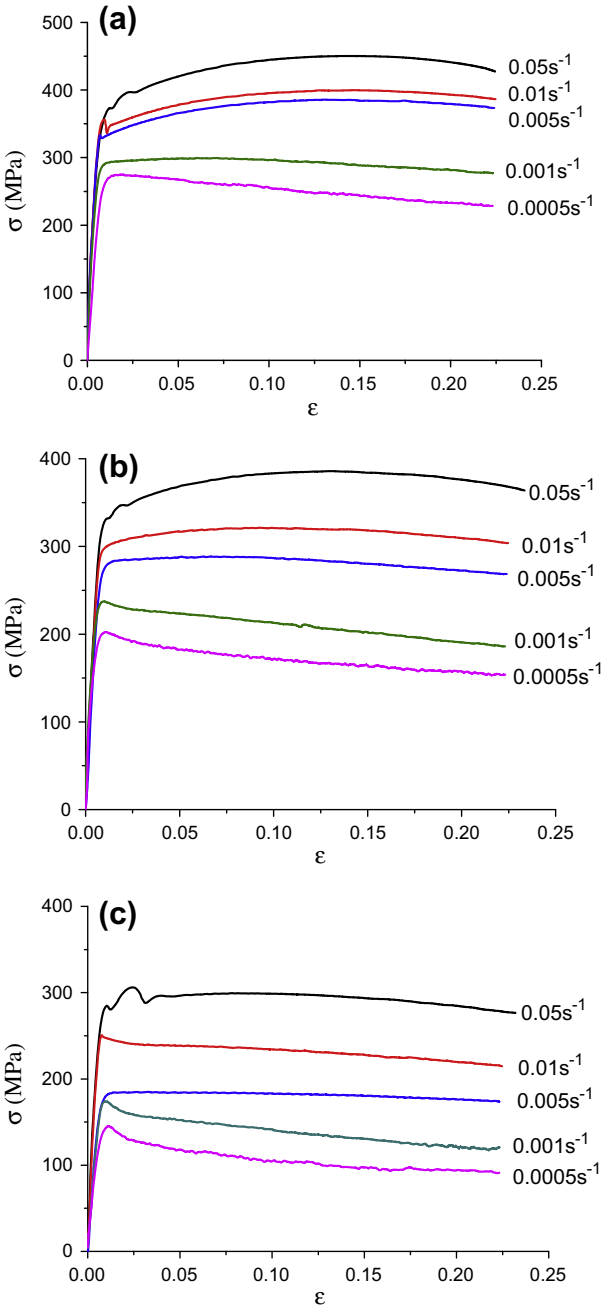

Fig. 2. True stress–strain curves of Ti–6Al–4V alloy under different experimental conditions: (a) 923 K; (b) 973 K and (c) 1023 K.

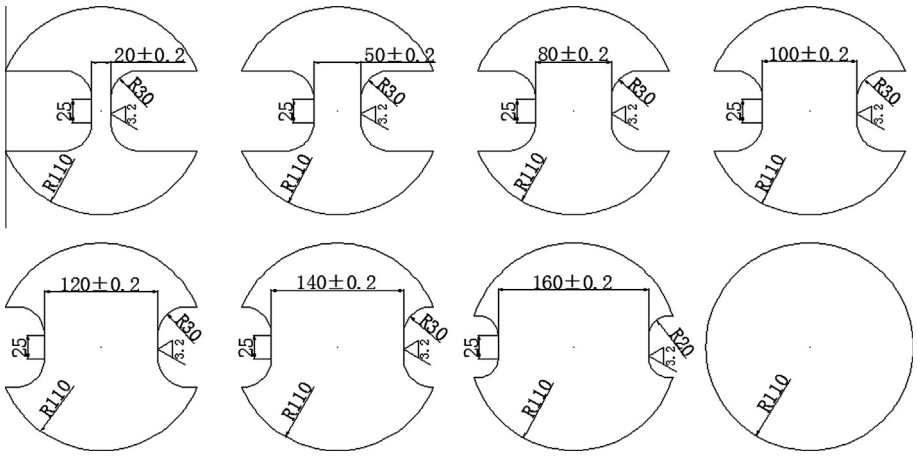

Fig. 3. Shapes and dimensions of specimens in hemispherical dome test.

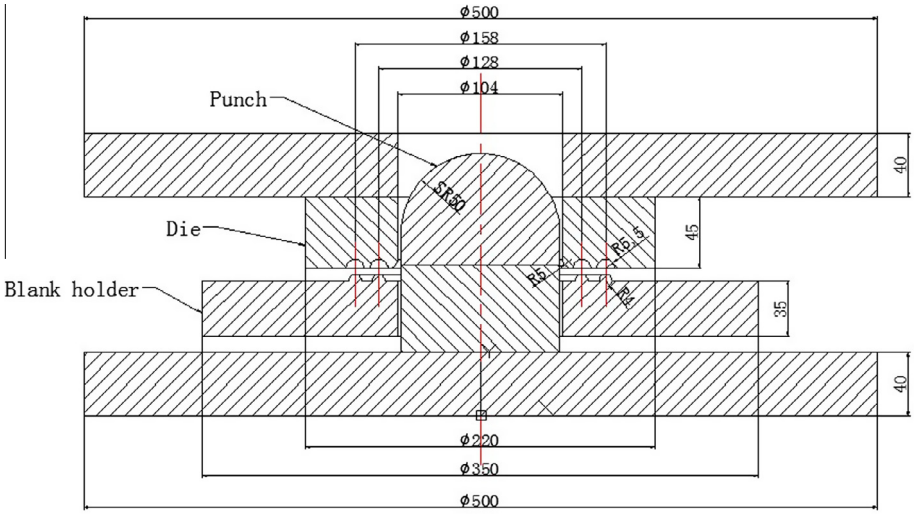

Fig. 4. Die assembly of hemispherical dome test at elevated temperature.

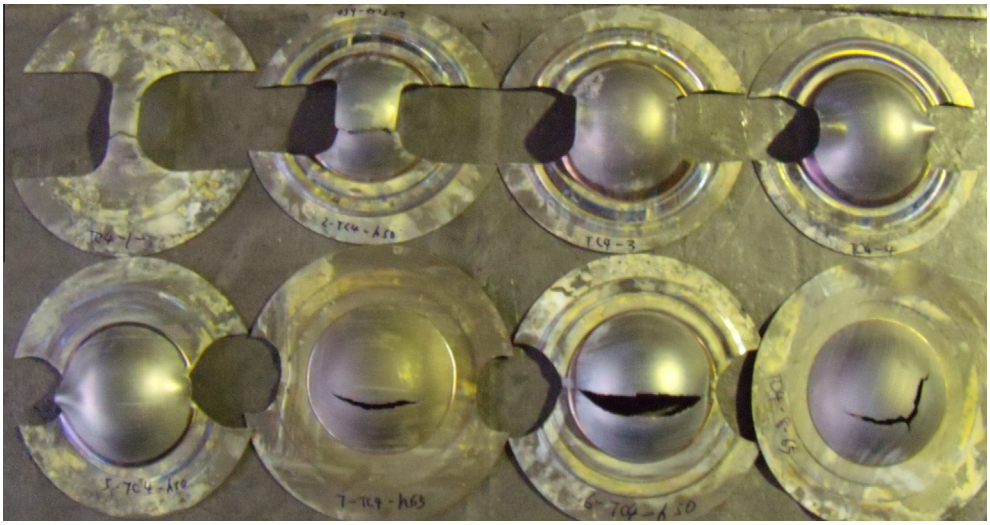

Fig. 5. Formed specimens of Ti–6Al–4V alloy-1.5 mm-973 K.

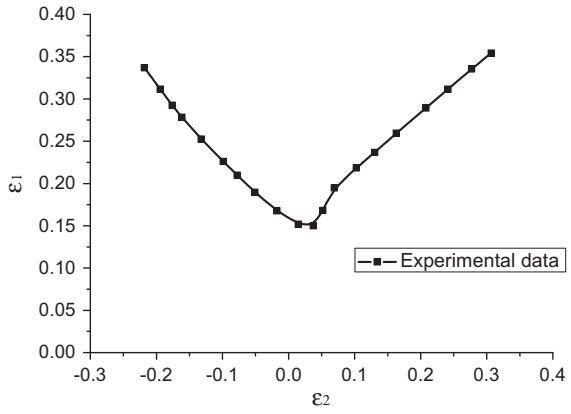

Fig. 6. Experimental FLC of Ti–6Al–4V alloy-1.5 mm-973 K.

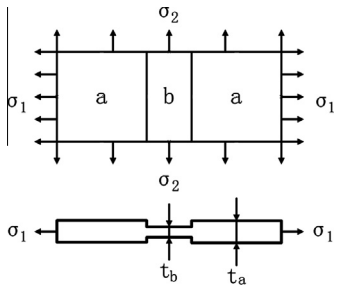

Fig. 7. M–K geometrical model.

2.2. Uniaxial tensile test at different strain-rates and temperatures

Fig. 2 presents the true stress–strain curves obtained from the uniaxial tensile tests [24]. The specimens were fabricated along rolling direction. Specimens with original gauge length of 25 mm and width of 12.5 mm were made by laser cutting. The uniaxial tensile tests were performed on a Zwick/Roell Z100 electric universal test machine. Prior to the tests, the specimens were heated to the deformation temperature and held at that temperature for at least 10 min to maintain the uniformity of temperature throughout the specimens. Then, the tests were carried out in the strain-rates range of 0.0005–0.05 s^{-1} and temperatures range of 923–1023 K.

2.3. Hemispherical dome test at elevated temperature

The FLC of Ti–6Al–4V alloy at 973 K was obtained by conducting the hemispherical dome test [25] on a 300 tons special thermal forming press. After cleaning the surfaces by Acetone, all the specimens were electro-etched using a grid of circles. Then, the surface, which touches with die, was coated with graphite for lubrication. The surface with printed grid was coated with boron nitride to prevent the titanium plate surface from oxidation. The die in the furnace cavity was heated to a specified temperature and the specimens were held at that temperature for at least 3 min to maintain the uniformity of temperature throughout the specimens. The test was then conducted with a constant forming speed of 1 m/min.

The shapes and dimensions of 1.5 mm thickness specimens are shown in Fig. 3. Die assembly is shown in Fig. 4. The material of die is 310S stainless steel, and the material of blank holder is 2Cr13.

The formed specimens are shown in Fig. 5. The strains were estimated by measuring the deformation of the grid as near as possible to the fracture zone, which are used to define the limit strains that sheet metal can reach. The experimental FLC is shown in Fig. 6.

Table 2
Value of K, n, m at different strain-rates and temperatures.

K	n	m	Temperature (K)	Strain-rate (s^{-1})
1552	−0.0628	0.2592	923	0.0005
1083	−0.0134	0.1946		0.001
716	0.0489	0.1006		0.005
607	0.0422	0.0759		0.01
567	0.0630	0.0397		0.05
1236	−0.0882	0.2881	973	0.0005
915	−0.0743	0.2393		0.001
626	−0.0115	0.1557		0.005
586	0.0098	0.1295		0.01
528	0.0386	0.0844		0.05
1421	−0.1522	0.3894	1023	0.0005
928	−0.1220	0.3179		0.001
928	−0.0048	0.1988		0.005
448	−0.0364	0.1626		0.01
393	−0.0051	0.1021		0.05

3. Constitutive model and forming limit prediction model

3.1. Constitutive model

In this paper, the variation in stress as a function of strain and strain-rate is described by the Backofen equation [26]:

$$\sigma = K\varepsilon^n \dot{\varepsilon}^m \tag{1}$$

The Von Mises yield criterion [27] is selected to calculate the FLC of Ti–6Al–4V alloy based on the M–K theory. In 1913, R. Von Mises proposed that the material begins plastic deformation as soon as the root-mean-square of the principal shear stress reaches a critical value in any stress state. This criterion applies only to isotropic materials:

$$\frac{1}{\sqrt{2}}\sqrt{(\sigma_1-\sigma_2)^2+(\sigma_2-\sigma_3)^2+(\sigma_3-\sigma_1)^2}=\sigma_s \tag{2}$$

3.2. Forming limit prediction model

The core of the M–K theory [28] is the hypothesis of inhomogeneous thickness which assumes that there is an initial groove on the surface of sheet metal. The localized instability is actually caused by the existence of inhomogeneous thickness [29].

The typical M–K geometrical model is shown in Fig. 7. Region a is the homogeneous area, and region b is the introduced non-homogeneous area, which is also called the groove portion.

The force equilibrium condition should be satisfied at the interface of regions a and b:

$$F_{1a} = F_{1b} \tag{3}$$

where F_{1a} and F_{1b} are the forces along the major stress of regions a and b, respectively.

The strain increments along the minor stress are the same on regions a and b:

$$d\varepsilon_{2a} = d\varepsilon_{2b} \tag{4}$$

Hence, Eq. (3) can be described as:

$$\sigma_{1a}\exp(\varepsilon_{3a}) = \sigma_{1b}\exp(\varepsilon_{3b})f_0 \tag{5}$$

where the initial thickness ratio f_0 is t_{b0}/t_{a0}. t_{a0} and t_{b0} are the initial thickness of regions a and b. ε_{3a} and ε_{3b} are the through-thickness strain of regions a and b.

φ is defined as the ratio of equivalent stress and major stress:

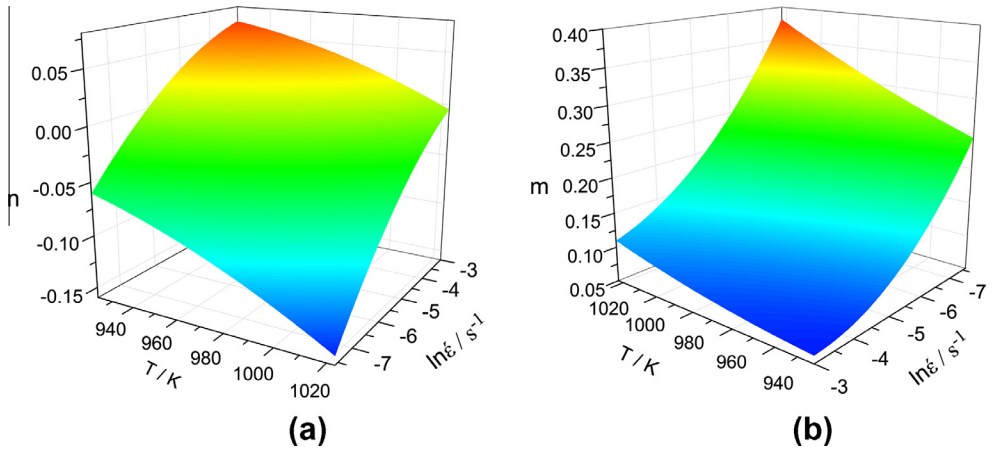

Fig. 8. Tendency of n-value and m-value along with strain-rate and temperature: (a) n-value and (b) m-value.

$$\varphi = \bar{\sigma}/\sigma_1 \tag{6}$$

Considering Eqs. (1) and (6), Eq. (5) can be written as:

$$\frac{1}{\varphi_a}\bar{\varepsilon}_a^n\dot{\bar{\varepsilon}}_a^m \exp(\varepsilon_{3a}) = \frac{f_0}{\varphi_b}\bar{\varepsilon}_b^n\dot{\bar{\varepsilon}}_b^m \exp(\varepsilon_{3b}) \tag{7}$$

where φ_a and φ_b are the ratio of equivalent stress and major stress of regions a and b. $\bar{\varepsilon}_a$ and $\bar{\varepsilon}_b$ are the equivalent strain of regions a and b. $\dot{\bar{\varepsilon}}_a$ and $\dot{\bar{\varepsilon}}_b$ are the equivalent strain-rate of regions a and b. n is the strain hardening exponent related to strain-rate and temperature. m is the strain-rate sensitivity parameter related to strain-rate and temperature. The value of n and m can be calculated by Eqs. (14) and (15) in Section 4.1 at a specific strain-rate and temperature.

α, ρ and β are defined as: α is the ratio of the minor stress and major stress. ρ is the ratio of the minor strain increments and the major strain increments. β is the ratio of the equivalent strain increments and the major strain increments.

$$\alpha = \sigma_2/\sigma_1 \tag{8}$$

$$\rho = d\varepsilon_2/d\varepsilon_1 = \dot{\varepsilon}_2/\dot{\varepsilon}_1 \tag{9}$$

$$\beta = d\bar{\varepsilon}/d\varepsilon_1 = \dot{\bar{\varepsilon}}/\dot{\varepsilon}_1 \tag{10}$$

The equivalent plastic work principle is as Eq. (11) under the condition of plane stress:

$$\bar{\sigma}\cdot d\bar{\varepsilon} = \sigma_1\cdot d\varepsilon_1 + \sigma_2\cdot d\varepsilon_2 \tag{11}$$

Eq. (12) can be deduced by combining Eqs. (6), (8), (9), (10) with Eq. (11):

$$\beta = (1+\alpha\rho)/\varphi \tag{12}$$

During the calculation procedure, the equivalent strain $\bar{\varepsilon}$ is continuously incremented by $\Delta\bar{\varepsilon}$. Then Eq. (7) can be written as Eq. (13) by combining Eqs. (4), (9), and (10):

$$\frac{1}{\varphi_a}(\bar{\varepsilon}_a+\Delta\bar{\varepsilon}_a)^n\left(\frac{\beta_a}{\rho_a}\right)^m \exp(\varepsilon_{3a}) = \frac{f_0}{\varphi_b}(\bar{\varepsilon}_b+\Delta\bar{\varepsilon}_b)^n\left(\frac{\beta_b}{\rho_b}\right)^m \exp(\varepsilon_{3b}) \tag{13}$$

The expression of ρ and φ which are needed in Eq. (13) can be calculated by Eq. (2).

When α and the equivalent strain increments of region a-$\Delta\bar{\varepsilon}_a$ are given ($\Delta\bar{\varepsilon}_a = 0.005$), the equivalent strain increments of region b-$\Delta\bar{\varepsilon}_b$ can be calculated by solving the nonlinear Eq. (13). The major and minor strain of region a is the forming limit strain when $\Delta\bar{\varepsilon}_{1b}/\Delta\bar{\varepsilon}_{1a} > 10$.

4. Results and discussion

4.1. Constitutive modeling

Nonlinear curve fitting is conducted on uniaxial tensile test data at the specific strain-rate and temperature. The values of K, n and m under different conditions are obtained from the fitting results, which are shown in Table 2.

The variation in K, n and m as a function of strain-rate and temperature are obtained by using nonlinear surface fitting. The fitting results are shown in Eqs. (14)–(16):

$$K = 2.0282\times10^4 - 36.8838x + 541.7598y + 0.0179x^2 + 60.8055y^2 - 0.0816xy \tag{14}$$

$$n = -2.9037 + 0.0066x - 0.0556y - 3.6794\times10^{-6}x^2 - 0.0036y^2 + 4.8210\times10^{-5}xy \tag{15}$$

$$m = 2.7583 - 0.0053x + 0.2242y + 2.7069\times10^{-6}x^2 + 0.0085y^2 - 1.8848\times10^{-4}xy \tag{16}$$

where x = T (temperature), $y = \ln\dot{\varepsilon}$.

Fig. 8 shows the tendency of n and m along with strain-rate and temperature within a certain range. The n-value increases with temperature lowering and strain-rate increasing. On the contrary, the m-value decreases with temperature lowering and strain-rate increasing.

The constitutive model with comprehensive consideration of strain-rate and temperature of Ti–6Al–4V alloy can be derived by Eqs. (1), (14), (15), (16). As shown below:

$$\sigma = K\varepsilon^n\dot{\varepsilon}^m$$

$$K = 2.0282\times10^4 - 36.8838x + 541.7598y + 0.0179x^2 + 60.8055y^2 - 0.0816xy$$

$$n = -2.9037 + 0.0066x - 0.0556y - 3.6794\times10^{-6}x^2 - 0.0036y^2 + 4.8210\times10^{-5}xy$$

$$m = 2.7583 - 0.0053x + 0.2242y + 2.7069\times10^{-6}x^2 + 0.0085y^2 - 1.8848\times10^{-4}xy$$

where $x = T$(temperature), $y = \ln\dot{\varepsilon}$. (17)

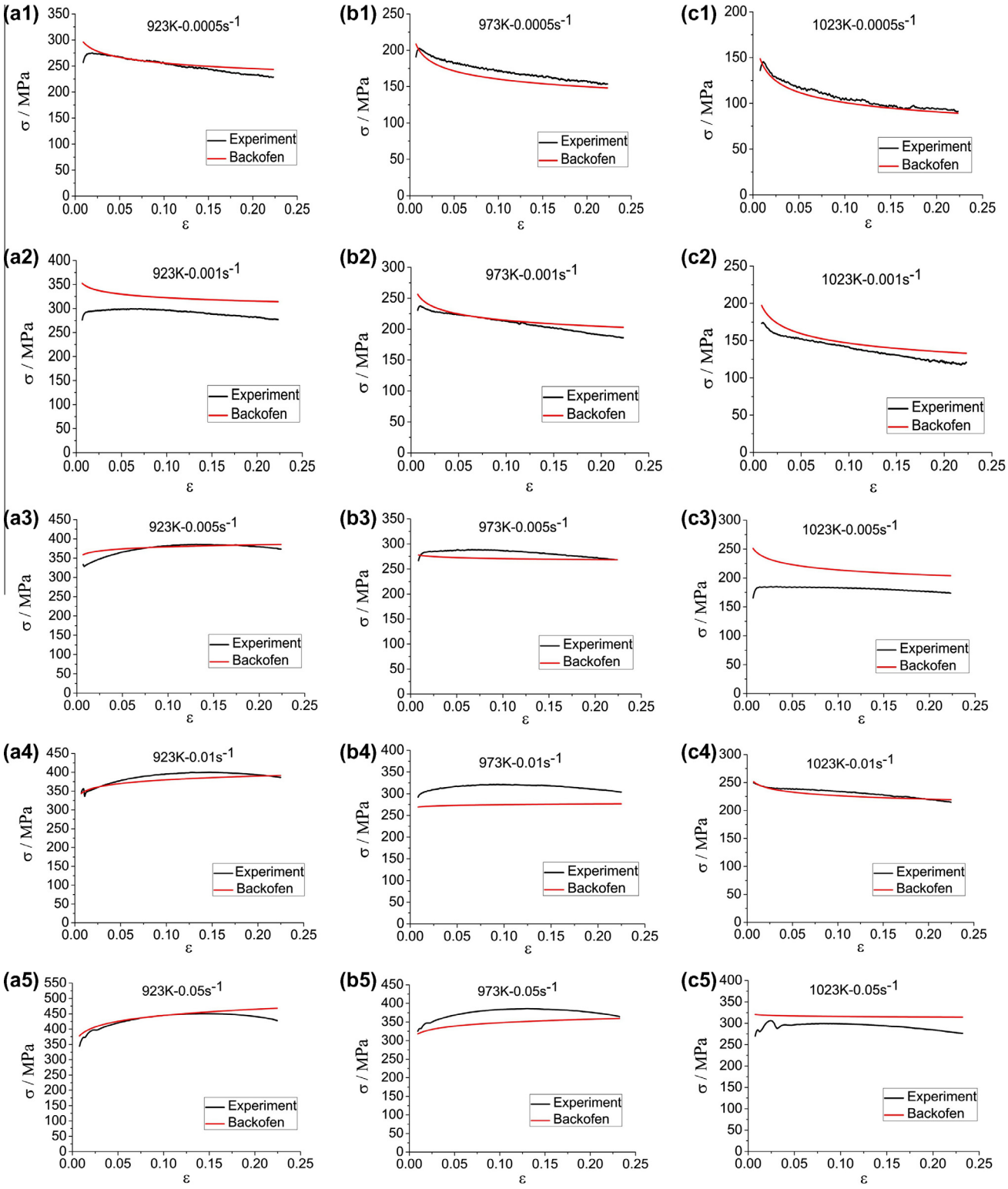

Fig. 9. Comparisons between the experimental and fitting stress–strain curves.

As seen from Fig. 9, the agreement between the experimental and predicted stress–strain curves is satisfactory. In order to compare the results statistically, the mean error is defined as:

$$\bar{e}_{ij} = \sum_{k=1}^{10} e_{ijk} \Big/ 10, \quad k \in N \tag{18}$$

where

$$e_{ijk} = |\sigma_p - \sigma_e|/\sigma_e \tag{19}$$

$\bar{e}_{ij}$ is the mean error of constitutive equation in a specific deformation condition; e_{ijk} is the error of constitutive equation at a fixed true strain in a specific deformation condition; σ_p is the predicted value from the constitutive equation; σ_e is the experimental value of the uniaxial tensile test; i is the temperature number, 1, 2, 3 corresponding to 923, 973, 1023 K; j is the strain rate number, 1, 2, 3, 4, 5 corresponding to 0.0005, 0.001, 0.005, 0.01, 0.05 s^{-1}; k is the

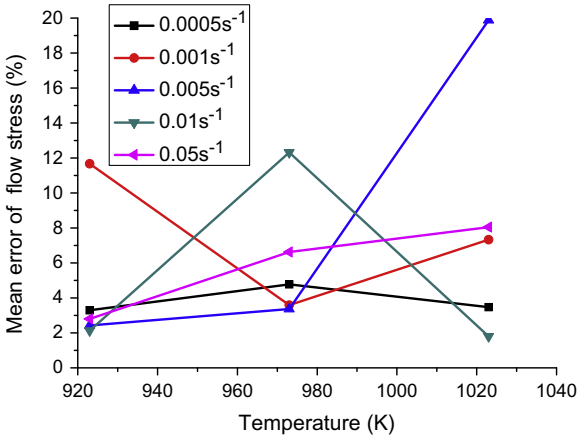

Fig. 10. Mean errors of flow stress varying with temperature and strain rate.

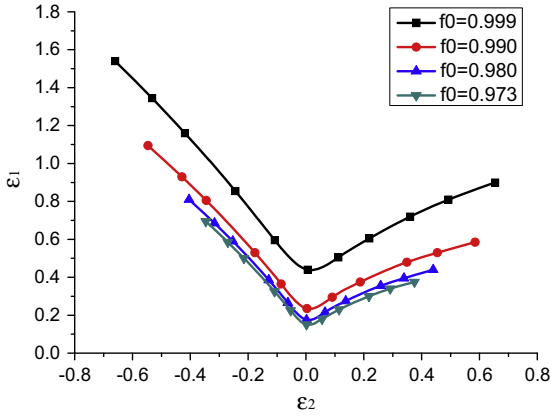

Fig. 11. Influence of initial thickness ratio on FLC.

strain number, 1, 2, 3, 4, 5, 6, 7, 8, 9, 10 corresponding to 0.01, 0.025, 0.05, 0.075, 0.1, 0.125, 0.15, 0.175, 0.2, 0.223.

Fig. 10 shows the mean errors of predicted flow stress in specific deformation conditions. The figure reveals that the mean errors are lower at relatively low temperatures than that at high temperatures. The majority of mean errors are below 8%, and the overall averaged mean error is 6.23%. The results indicate that the established constitutive model is satisfactory, and can be used to predict the flow stress of Ti–6Al–4V alloy at elevated temperature.

4.2. Influence of strain-rate and temperature on forming limit prediction

In the process of theoretical prediction of FLC, the limit strains are greatly affected by the value of the initial thickness ratio (f_0). The curves plotted in Fig. 11 were performed using $n = 0.0382$ and $m = 0.0793$. The limit strain decreases with decreasing value of f_0 untill a particular location corresponds to a constant value of f_0.

In many investigations [19,30,31], f_0 is used as an adjustable parameter in the M–K analysis to match the calculated FLD_0, which is the limit strain at the plane strain condition, with the experimental data. In the calculation, the initial thickness ratio was assumed as $f_0 = 0.973$.

In order to reveal the effect of the strain-rate on FLC, the theoretical FLC at different strain-rates are compared in Fig. 12. The result shows that the effect of the strain-rate on FLC exhibits the

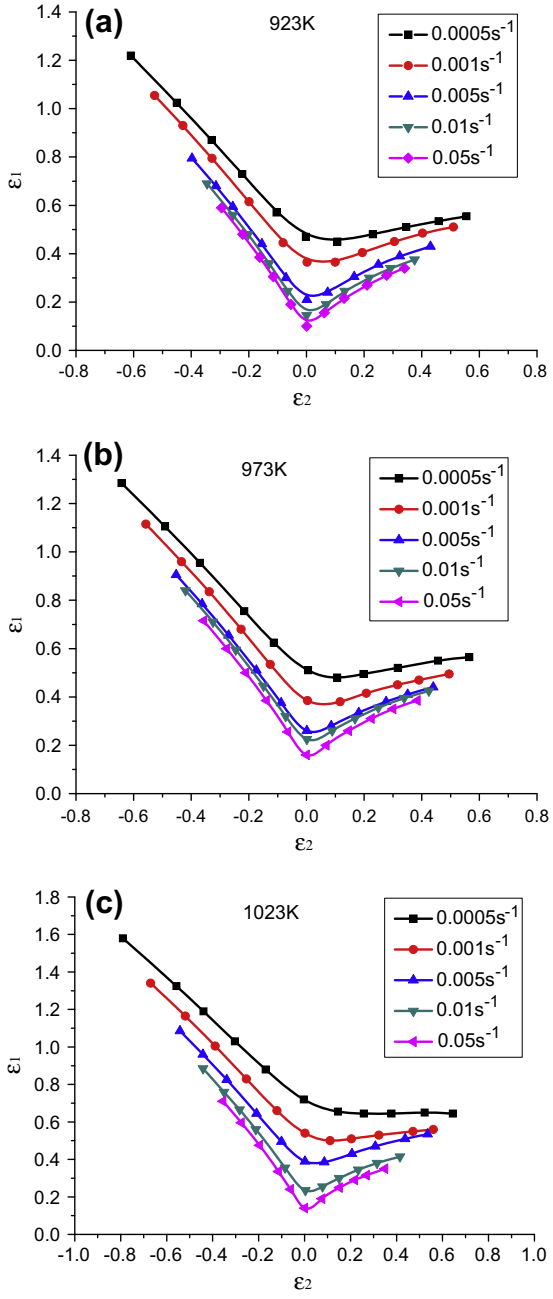

Fig. 12. Influence of strain-rate on FLC at different temperatures: (a) 923 K; (b) 973 K and (c) 1023 K.

same tendency at each specific temperature. The fact that the limit strain decreases with strain-rate increasing is obvious. Furthermore, the effect of strain-rate on the FLC becomes stronger with temperature increasing. At 923 K, the limit strain under plane strain condition decreases from 0.48 to 0.12 with the strain-rate increasing from 0.0005 to 0.05 s^{-1}. At 1023 K, it decreases from 0.73 to 0.16. As a result, reducing the strain-rate is helpful to improve the formability of Ti–6Al–4V alloy, especially at elevated temperature. Similar results were reported by Domiaty [32], where the FLD was predicted by theoretical calculation. The results also indicated that the level of the FLC increases with decrease in strain-rate.

As shown in Fig. 13, the theoretical FLCs at three different temperatures are compared in order to reveal the effect of temperature on FLC. From the comparison, it can be concluded that the limit

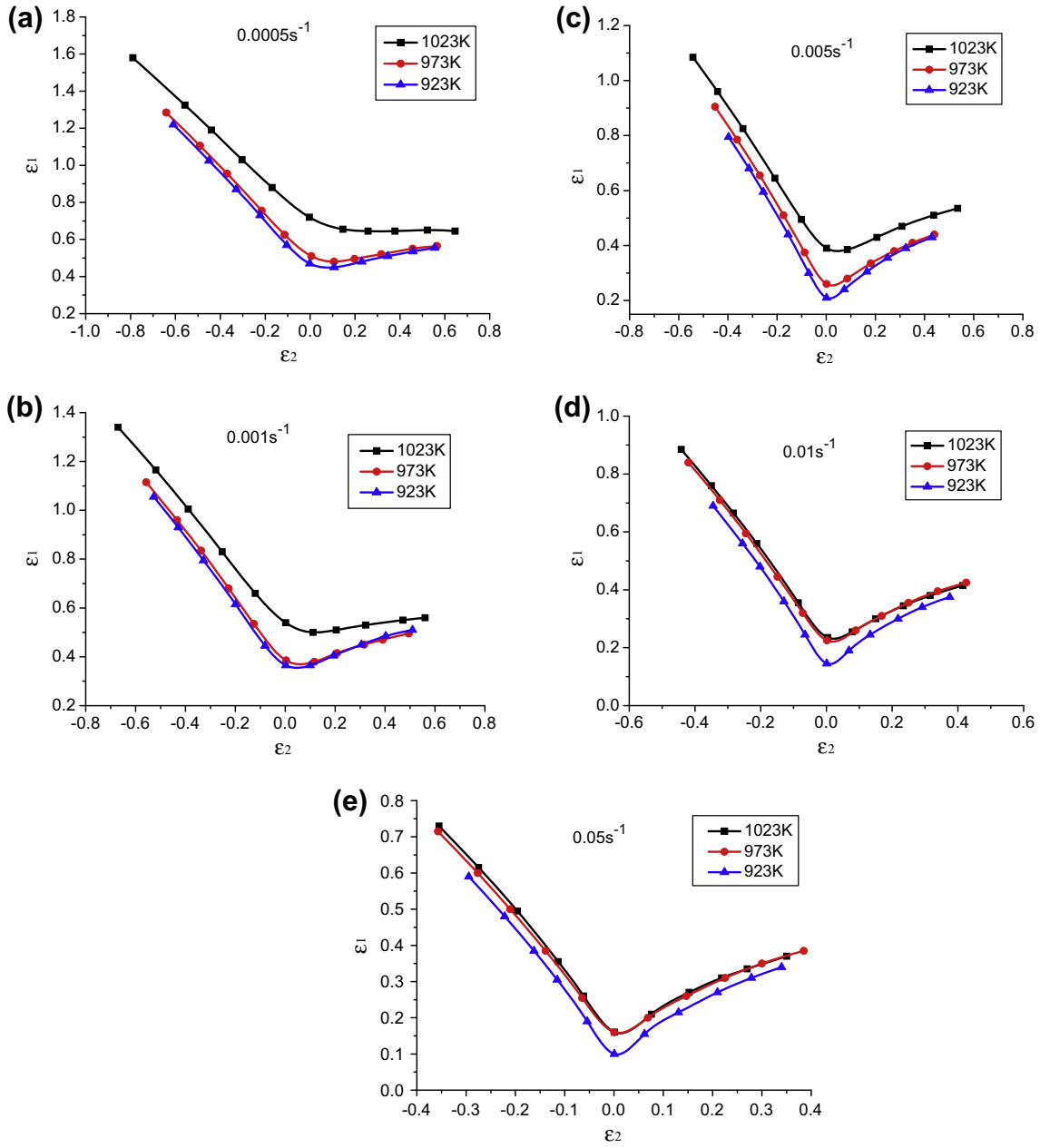

Fig. 13. Influence of temperature on FLC at different strain-rates: (a) 0.0005 s^{-1}; (b) 0.001 s^{-1}; (c) 0.005 s^{-1}; (d) 0.01 s^{-1} and (e) 0.05 s^{-1}.

strain increases with temperature increasing. Furthermore, the effect of temperature on the FLC becomes stronger with strain-rate decreasing. At 0.0005 s^{-1}, the limit strain under plane strain condition increases from 0.48 to 0.73 with the temperature increasing from 923 K to 1023 K. At 0.05 s^{-1}, it increases from 0.12 to 0.16. So a relatively high deformation temperature is helpful to improve the formability of Ti–6Al–4V alloy, especially at low strain-rate. Similar results were reported by Cheng [11] and Lai [12], where the formability of Ti–6Al–4V was evaluated by Limiting Dome Height (LDH) of specimens in Swift forming test at various temperatures. The results revealed that the values of LDH linearly increased with increasing temperature. Also, the FLDs of Ti–6Al–4V were obtained by experiments conducted at different temperature in the study of Odenberger et al. [14]. The result indicated that the formability of Ti–6Al–4V increases with the temperature increasing.

4.3. Experimental verification of forming limit prediction

The theoretical FLCs are compared with the experimental FLC under the same condition in order to verify the reliability and robustness of the theoretical prediction.

As shown in Fig. 14, the theoretical FLCs based on M–K theory along with Von Mises yield criterion agree very well with the experimental FLC in the positive minor strain region. But in the negative minor strain region, the theoretical FLCs are higher than the experimental FLC. For statistical comparison, the relative error is defined as:

$$e_k = |\varepsilon_{1p} - \varepsilon_{1e}|/\varepsilon_{1e}, \quad k \in N \tag{20}$$

e_k is the relative error of forming limit prediction model; ε_{1p} is the predicted value from the forming limit prediction model; ε_{1e} is the

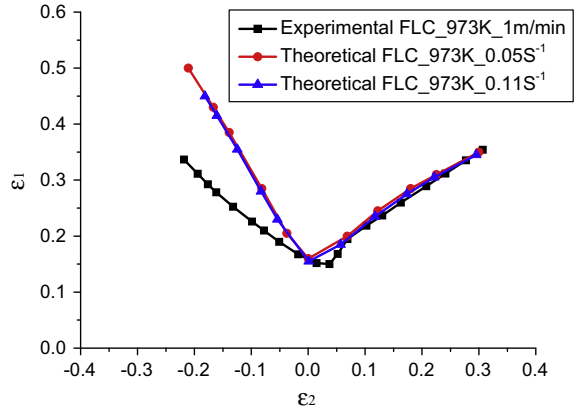

Fig. 14. Comparison between theoretical prediction and experimental measurement of FLC.

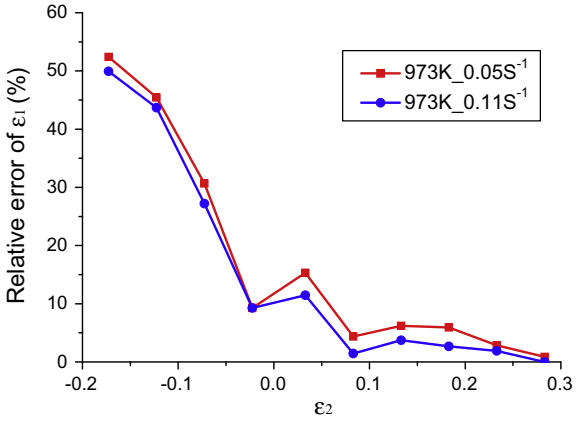

Fig. 15. Relative error of major strain varying with minor strain.

experimental value of the hemispherical dome test; k is the minor strain number, 1, 2, 3, 4, 5, 6, 7, 8, 9, 10 corresponding to −0.173, −0.123, −0.073, −0.023, 0.033, 0.083, 0.133, 0.183, 0.233, 0.283.

Fig. 15 presents the distribution of relative errors.

In this paper, the theoretical prediction of FLC is based on the typical M–K model, which assumes the pre-existing inhomogeneous thickness is in the form of a groove. The groove is perpendicular to the major strain direction. Actually, in the negative minor strain region of FLD, the angle between the groove and the major strain direction is mutative at each increment of the plastic deformation. The limit strains are sensitive to the angle [33]. As a result, the assumption of normality between the groove and the major strain direction is a severe restriction and leads to inaccurate prediction of the FLD in the negative minor strain region.

In further research, the angle between the groove and the major strain direction will be considered as part of the calculation of FLC. The influence of the angle on FLC will be discussed in detail.

5. Conclusions

Thermo-mechanical response of Ti–6Al–4V alloy was studied via a set of uniaxial tensile tests. The FLD of Ti–6Al–4V alloy was investigated from the perspective of theoretical calculation and experimental measurement. The primary conclusions are summarized below.

(1) The constitutive model considering the strain-rate and temperature effect was established by researching the deformation rule of Ti–6Al–4V alloy at different strain-rates and temperatures. The tendency of strain hardening exponent n and strain-rate sensitivity parameter m in the constitutive model along with strain-rate and temperature was revealed.

(2) The FLC of Ti–6Al–4V alloy at the temperature of 972 K was measured by conducting the hemispherical dome test with specimens of different widths.

(3) The forming limit prediction model of Ti–6Al–4V alloy, which takes strain-rate and temperature sensitivity into account, was predicted based on M–K theory along with Von Mises yield criterion. The theoretical FLCs of Ti–6Al–4V at different strain-rates and temperatures were predicted.

(4) The limit strain of Ti–6Al–4V alloy decreases with strain-rate increasing and temperature lowering. Furthermore, the effect of the strain-rate on the FLC becomes stronger with temperature increasing. The effect of temperature on the FLC becomes stronger with strain-rate decreasing.

(5) The comparison between the theoretical FLC and the experimental FLC shows that the method considering the strain-rate and temperature effect to predict limit strains in the positive minor strain region of FLD is accurate and reliable.

Acknowledgements

The paper is supported by National Natural Science Foundation of China (51175022) and National Defense Pre-research Program of China (51318040315).

References

[1] Pittsburgh: RTI International Metals, Inc; 2000-12. Available from: <http://rtiintl.com/en-us/markets/Pages/aerospace.aspx>.
[2] Khan AS, Yu SJ. Deformation induced anisotropic responses of Ti–6Al–4V alloy. Part I: experiments. Int J Plast 2012;38:1–13.
[3] Khan AS, Yu SJ, Liu HW. Deformation induced anisotropic responses of Ti–6Al–4V alloy Part II: a strain rate and temperature dependent anisotropic yield criterion. Int J Plast 2012;38:14–6.
[4] Beal JD, Boyer R, Sanders D, The boeing company. forming of titanium and titanium alloys. In: Semiatin SL, editor. ASM Handbook, Volume 14B: Metalworking: Sheet forming. ASM, International; 2006. p. 656–69.
[5] Stoughton TB. A general forming limit criterion for sheet metal forming. Int J Mech 2000;42:1–27.
[6] Lang R, Hofmann K, Gese H. Cold forming of beta titanium sheet. In: RTO AVT specialists' meeting on cost effective application of titanium alloys in military platforms, Loen, Norway; May 7–11, 2001.
[7] Jurendić S, Gaiani S. Deep drawing simulation of α-titanium alloys using LS-Dyna. In: 8th European LS-DYNA Users Conference, Strasbourg; May 2011.
[8] Esfahlan HN, Dizaji SA, Djavanroodi F. Experimental and numerical analysis for hydro forming of Ti6Al4V alloy used in aerospace, assisted by floating disk. J Appl Sci 2009;9(16):2925–32.
[9] Satoh J, Gotoh M, Maeda Y. Stretch-drawing of titanium sheets. J Mater Process Technol 2003;139:201–7.
[10] Lai CP, Chan LC, Chow CL. Effects of tooling temperatures on formability of titanium TWBs at elevated temperatures. J Mater Process Technol 2007;191:157–60.
[11] Cheng CH, Chan LC, Lai CP, Chow CL. Formability of Ti-TWBs at elevated temperatures. In: SAE international congress. SAE paper no. 2006-01-0353, Detroit; April 3–6 2006.
[12] Chen FK, Chiu KH. Stamping formability of pure titanium sheets. J Mater Process Technol 2005;170:181–6.
[13] Lai CP, Chan LC, Chow CL, Yu KM. Thermal forming of light-weight alloys under a multi-stage forming process. Proc Instn Mech Eng, Part C: J Mech Eng Sci 2010;224:797–803.
[14] Odenberger EL, Hertzman J, Thilderkvist P, Merklein M, Kuppert A, Stöhr T, et al. Thermo-mechanical sheet metal forming of aero engine components in Ti–6Al–4V-Part 1: Material characterization. Int J Mater Form 2012.
[15] Odenberger EL, Pederson R, Oldenburg M. Thermo-mechanical material response and hot sheet metal forming of Ti-6242. Mater Sci Eng A 2008;489:158–68.
[16] Rocha ABD, Santos AD, Teixeira P, Butuc MC. Analysis of plastic flow localization under strain paths changes and its coupling with finite element simulation in sheet metal forming. J Mater Process Technol 2009;209:5097–109.
[17] Khafri MA, Mahmudi R. Predicting of plastic instability and forming limit diagrams. Int J Mech 2004;46:1289–306.

[18] Min JY, Lin JP, Li JY, Bao WH. Investigation on hot forming limits of high strength steel 22MnB5. Compos Mater Sci 2010;49:326–32.
[19] Zhang CS, Leotoing L, Guines D, Ragneau E. Theoretical and numerical study of strain rate influence on AA5083 formability. J Mater Process Technol 2009; 209:3849–58.
[20] Khan AS, Baig M. Anisotropic responses, constitutive modeling and the effects of strain-rate and temperature on the formability of an aluminum alloy. Int J Plast 2011;27:522–38.
[21] Haghdadi N, Zarei-Hanzaki A, Abedi HR. The flow behavior modeling of cast A356 aluminum alloy at elevated temperatures considering the effect of strain. Mater Sci Eng A 2012;535:252–7.
[22] Haghdadi N, Zarei-Hanzaki A, Khalesian AR, Abedi HR. Artificial neural network modeling to predict the hot deformation behavior of an A356 aluminum alloy. Mater Des 2013;49:386–91.
[23] Xiao J, Li DS, Li XQ, Deng TS. Constitutive modeling and microstructure change of Ti–6Al–4V during the hot tensile deformation. J Alloys Compd 2012;541: 346–52.
[24] ISO 6892-2. Metallic materials-tensile testing-Part2: method of test at elevated temperature. Case Postale, Geneva: International Organization for Standardization; 2011.
[25] ISO 12004-2. Metallic materials-sheet and strip-determination of forming-limit curves-Part 2: determination of forming-limit curves in the la boratory. Case Postale, Geneva: International Organization for Standardization; 2008.
[26] Lin YC, Chen XM. A critical review of experimental results and constitutive descriptions for metals and alloys in hot working. Mater Des 2011;32: 1733–59.
[27] Zhu XK, Leis BN. Average shear stress yield criterion and its application to plastic collapse analysis of pipelines. Int J Pres Ves Pip 2006;83: 663–71.
[28] Marciniak Z, Kuczynski K. Limit strains in the processes of stretch-forming sheet metal. Int J Mech 1967;9:609–12 [IN1-IN2, 613–20].
[29] Nurcheshmeh M, Green DE. Prediction of sheet forming limits with Marciniak and Kuczynski analysis using combined isotropicnonlinear kinematic hardening. Int J Mech 2011;53:145–53.
[30] Naka T, Torikai G, Hino R, Yoshida F. The effects of temperature and forming speed on the forming limit diagram for type 5083 aluminum–magnesium alloy sheet. J Mater Process Technol 2001;113:648–53.
[31] Soare SC. Theoretical considerations upon the MK model for limit strains prediction: the plane strain case, strain-rate effects, yield surface influence, and material heterogeneity. Eur J Mech A – Solid 2010;29:938–50.
[32] Domiaty AE. The effect of strain, strain rate and temperature on formability of Ti–6Al–4V alloy. J Mater Process Technol 1992;32:243–51.
[33] Allwood JM, Shouler DR. Generalised forming limit diagrams showing increased forming limits with non-planar stress states. Int J Plast 2009; 25:1207–30.